

Direct Detection of Bound Ammonium Ions in the Selectivity Filter of Ion Channels by Solid-State NMR

Carl Öster, Kumar Tekwani Movellan, Benjamin Goold, Kitty Hendriks, Sascha Lange, Stefan Becker, Bert L. de Groot, Wojciech Kopec, Loren B. Andreas, and Adam Lange*



Cite This: *J. Am. Chem. Soc.* 2022, 144, 4147–4157



Read Online

ACCESS |



Metrics & More

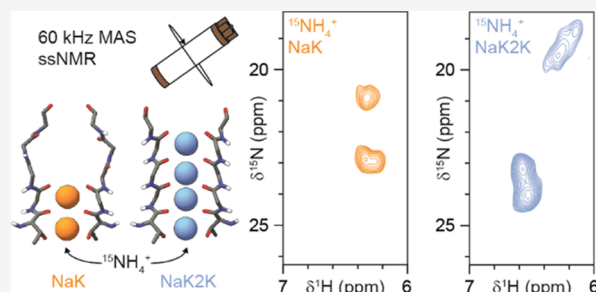


Article Recommendations



Supporting Information

ABSTRACT: The flow of ions across cell membranes facilitated by ion channels is an important function for all living cells. Despite the huge amount of structural data provided by crystallography, elucidating the exact interactions between the selectivity filter atoms and bound ions is challenging. Here, we detect bound ^{15}N -labeled ammonium ions as a mimic for potassium ions in ion channels using solid-state NMR under near-native conditions. The non-selective ion channel NaK showed two ammonium peaks corresponding to its two ion binding sites, while its potassium-selective mutant NaK2K that has a signature potassium-selective selectivity filter with four ion binding sites gave rise to four ammonium peaks. Ions bound in specific ion binding sites were identified based on magnetization transfer between the ions and carbon atoms in the selectivity filters. Magnetization transfer between bound ions and water molecules revealed that only one out of four ions in the selectivity filter of NaK2K is in close contact with water, which is in agreement with the direct knock-on ion conduction mechanism where ions are conducted through the channel by means of direct interactions without water molecules in between. Interestingly, the potassium-selective ion channels investigated here (NaK2K and, additionally, KcsA-Kv1.3) showed remarkably different chemical shifts for their bound ions, despite having identical amino acid sequences and crystal structures of their selectivity filters. Molecular dynamics simulations show similar ion binding and conduction behavior between ammonium and potassium ions and identify the origin of the differences between the investigated potassium channels.



INTRODUCTION

Ion channels are essential for living cells due to their role in electric signaling, which is important for many biological functions. Since ions cannot permeate lipophilic cell membranes, they must enter and leave cells through protein channels that are embedded into the membrane. Dysfunctional ion channels in humans are known to be involved in various neurological diseases such as epilepsy or autism. Because of their involvement in a wide variety of physiological processes, ion channels are well known to be important drug targets.¹ NaK is a bacterial non-selective ion channel that conducts both sodium (Na^+) and potassium (K^+) ions.² Because of its similarity to human cyclic nucleotide-gated ion channels, NaK has become an important model system for non-selective ion channels. NaK is a tetrameric protein in which each monomer consists of two transmembrane helices connected by an intramembrane pore helix and a six-amino-acid-long selectivity filter (SF), TVGDGN. NaK2K, a double mutant (D66Y, N68D) of NaK, is K^+ -selective and has become an established model system for K^+ -selective ion channels.^{3–5} NaK2K is very similar to KcsA, the most studied K^+ -selective ion channel, for which the crystal structure marked an important breakthrough in ion channel research.⁶ The SF of KcsA was revealed as a

narrow pore with four ion binding sites (called S1 to S4) made up of the backbone carbonyls of five amino acids (TVGYG) and the side chain of the threonine.

Although many studies using a range of structural methods have focused on investigating ion conduction in K^+ -selective ion channels, the exact mechanism is still debated.^{7,8} Originally, it was proposed that water molecules and K^+ ions permeate together in an alternating arrangement (water, ion, water, ion) through the SF.⁹ This was the accepted model in the field until 2014 when molecular dynamics (MD) simulations and reanalysis of the crystal structures led to a new model suggesting that ions are in direct contact with each other and no water molecules are co-transported during the conduction process.¹⁰ Since then, several techniques including 2D infrared spectroscopy¹¹ and anomalous X-ray diffraction¹² have been interpreted in favor of each of the suggested models.

Received: December 20, 2021

Published: February 24, 2022



In a recent solid-state NMR study, we showed, by investigating H/D exchange and water-to-amide spin diffusion (SD) experiments, that no water could be detected in the SF of NaK2K when K^+ ions were present.¹³ It is therefore interesting to now investigate ion conduction from the perspective of the ions. K^+ ions can in principle be detected in NMR experiments using the NMR active nucleus ^{39}K . Unfortunately, ^{39}K has a rather low gyromagnetic ratio and it is a quadrupolar nucleus, making it very challenging for protein NMR. An attractive mimic for K^+ ions is ^{15}N -labeled ammonium ions ($^{15}NH_4^+$) that contain two NMR active nuclei (1H and ^{15}N) and allow for detection of the very sensitive 1H nucleus. $^{15}NH_4^+$ ions have been used as a mimic for K^+ ions in solution NMR studies of several different biological systems.^{14,15} Recently, a solution NMR study of KscA with $^{15}NH_4^+$ ions showed five different resonances originating from $^{15}NH_4^+$ ions.¹⁶ The peaks were attributed to bound ions in sites S1 to S4 and the presence of an ion in the S0 site above the SF. However, this assumption was not confirmed by transfers between ions and atoms in the protein.

Here, we used 1H -detected solid-state NMR on ion channel proteins embedded in a lipid bilayer. This enables the detailed analysis of the structure and dynamics of membrane proteins under near-to-physiological conditions.^{17–23} We were able to detect $^{15}NH_4^+$ ions bound in the SF of the non-selective ion channel NaK, its K^+ -selective mutant NaK2K, and KcsA-Kv1.3,²⁴ a mutant of KcsA resembling the human voltage-gated channel Kv1.3. Importantly, by transferring magnetization between $^{15}NH_4^+$ ions and backbone atoms of the SF residues, we could assign ions bound in specific ion binding sites. Additionally, we investigated interactions between bound $^{15}NH_4^+$ ions and water molecules and studied the effect $^{15}NH_4^+$ ions have on the investigated proteins compared to K^+ ions. Finally, we performed MD simulations to investigate the behavior of NH_4^+ ions compared to K^+ ions during conduction events.

EXPERIMENTAL SECTION

Sample Preparation. NaK and NaK2K were expressed and purified as previously described.^{13,25} Briefly, both the NaK and NaK2K constructs are missing the first 19 amino acids and have a C-terminal hexahistidine tag. The NaKΔ19 construct in a pQE60 vector was expressed in *Escherichia coli* NEB Express I⁹. The NaK2KΔ19 construct (in a pET28a vector) was expressed in *E. coli* OverExpress C43(DE3). Both were expressed in deuterated minimal media supplemented with $^{13}C_6$ -D-glucose and $^{15}NH_4Cl$, and cells were adapted to D_2O conditions. The fully protonated NaK2KΔ19 was expressed in minimal media supplemented with $^{13}C_6$ -D-glucose and $^{15}NH_4Cl$. The deuterated samples were solubilized with 80 mM DM (*n*-decyl- β -maltoside, Glycon Biochemicals) and the protonated samples with 40 mM DM in the solubilization buffer. The deuterated samples were dialyzed against the sample buffer [100% H_2O with 20 mM tris (pH 8) and 50 mM $^{15}NH_4Cl$] for 8 days at a 100 \times dilution factor. The fully protonated sample was dialyzed initially against 20 mM tris (pH 8) for 2 days with a 100 \times dilution factor, after which it was dialyzed against 20 mM tris (pH 8) with 50 mM $^{15}NH_4Cl$ for the remaining 6 days. During dialysis, the protein was reconstituted into an *E. coli* total lipid extract (100500, Avanti Polar Lipids) in a protein/lipid ratio of 2:1 (w/w).

The deuterated samples were washed under different ionic conditions. Two batches of deuterated NaK2K were prepared. One batch was washed from 50 mM $^{15}NH_4Cl$ to a buffer without cations and back to 50 mM $^{15}NH_4Cl$. The second batch was washed from 50 mM $^{15}NH_4Cl$ to a buffer without cations and finally to 50 mM KCl. For NaK, one batch was sufficient for all washes. The sample was

washed from 50 mM $^{15}NH_4Cl$ to a buffer without cations, back to 50 mM $^{15}NH_4Cl$, and finally to 50 mM KCl. The washing procedure consisted of ultracentrifugation of the sample at 100,000 relative centrifugal force for 1 h, removal of the original sample buffer, and addition of the new sample buffer. This procedure was repeated 2 to 3 times during each wash, with the sample rotating at 4 °C between the buffer exchange steps. The total washing time was 7–14 days for each buffer exchange. A short total washing time was used when cations were introduced, and a long washing time was used when the samples were washed to a buffer without cations.

KcsA-Kv1.3 was expressed and purified as previously described.²⁴ Briefly, plasmid pQE32-Kc1.3 ChiIV L90C coding for KcsA-Kv1.3 was transformed into *E. coli* strain M15 (Prep4) (Qiagen). To obtain uniformly $^{15}N^{13}C$ -labeled protein, cells were grown at 37 °C in an 8 L minimal media-shaking culture until an OD_{600} of 0.75 was achieved. The cells were pelleted, washed with 2 L of 5 \times M9 salts, and dissolved in 2 L of minimal media with 1 g of $^{15}NH_4Cl$ per liter as a nitrogen source and 4 g of $^{13}C_6$ -D-glucose per liter as a carbon source. After 1 h of shaking at 25 °C, protein expression was induced by adding 0.8 mM IPTG. The cells were harvested 3.5 h after induction. The cells were dissolved in 250 mL of lysis buffer (50 mM MOPS, pH 7.2, 150 mM KCl, complete EDTA-free, 200 mM PMSF) and lysed by three passages through a French press. From the pellet, the protein was solubilized in 100 mL of 100 mM Na-phosphate, pH 7.0, 150 mM KCl, and 40 mM DM (Anatrace) by overnight incubation at 4 °C. From the supernatant, the protein was purified by Ni-NTA chromatography²⁶ using 2 mL of Ni-NTA agarose (Qiagen). The protein was eluted from the Ni-NTA agarose with 100 mM Na-phosphate, pH 7.8, 150 mM KCl, 400 mM imidazole, and 4 mM DM. The elution fractions were combined, and the buffer was exchanged against 50 mM Na-phosphate, pH 7.4, 50 mM NaCl, and 4 mM DM using a HiPrep 26/10 desalting column (Amersham). The final protein concentration was determined with the Bio-Rad DC protein assay. The protein was reconstituted into aolectin from soybean (Sigma) at a 100/1 aolectin/KcsA-Kv1.3 molar ratio, removing the detergent with Bio-Beads (Bio-Rad). The liposomes with the reconstituted protein were washed several times in 50 mM Na-phosphate, pH 7.4, and 50 mM NaCl.

Reconstituted KcsA-Kv1.3 was pelleted and resuspended in 50 mM phosphate buffer solution at pH 7, containing 50 mM NaCl and 50 mM KCl. KCl exchange against 150 mM $^{15}NH_4Cl$ was performed directly by incubating the 0.7 mm rotor with an excess of 50 mM phosphate, 50 mM NaCl, and 150 mM $^{15}NH_4Cl$ at pH 7. Briefly, the drive cap was removed from the 0.7 mm rotor, and the rotor was incubated at room temperature with 200 μ L of 50 mM phosphate, 50 mM NaCl, and 150 mM $^{15}NH_4Cl$ at pH 7. The buffer was renewed every 24 h for 4 days. To ensure buffer exchange in such a small rotor diameter, the 0.7 mm rotor was transferred into a 1.3 mm rotor and centrifuged using a benchtop centrifuge at every buffer renewal.

Solid-State NMR. The fully protonated $^{13}C^{15}N$ -labeled NaK2K was initially packed into a 3.2 mm rotor. ^{13}C -detected NCO and NCA spectra were recorded on a spectrometer with an external magnetic field strength corresponding to a 1H Larmor frequency of 800 MHz (Bruker), equipped with a 3.2 mm E-free probe (Bruker BioSpin) operating at 11 kHz MAS and at a sample temperature of 10 °C. The sample was then transferred to a 0.7 mm rotor using a micro spatula. 1H -detected solid-state NMR experiments of the fully protonated $^{13}C^{15}N$ -labeled NaK2K sample with 50 mM $^{15}NH_4Cl$ were performed on a spectrometer with an external magnetic field strength corresponding to a 1H Larmor frequency of 900 MHz (Bruker) using a 0.7 mm probe (Bruker BioSpin) operating at 100 kHz MAS and at a sample temperature of 25 °C. To compensate for the drift of the magnetic field, an external lock was used. Five 3D experiments were recorded for assignments: CP-based (H)C α NH, (H)C α (CO)-NH, (H)CONH, (H)COC α H α , and a (H)CCH TOCSY with 15 ms ^{13}C – ^{13}C DIPSI-3 mixing at a nutation frequency of 10 kHz. All deuterated $^{13}C^{15}N$ -labeled samples were packed into 1.3 mm rotors. A silicone-based glue was used to seal the rotors to prevent leakage and drying out of the samples. Experiments were recorded at 60 kHz MAS and at a sample temperature of 25 °C using 1.3 mm probes (Bruker

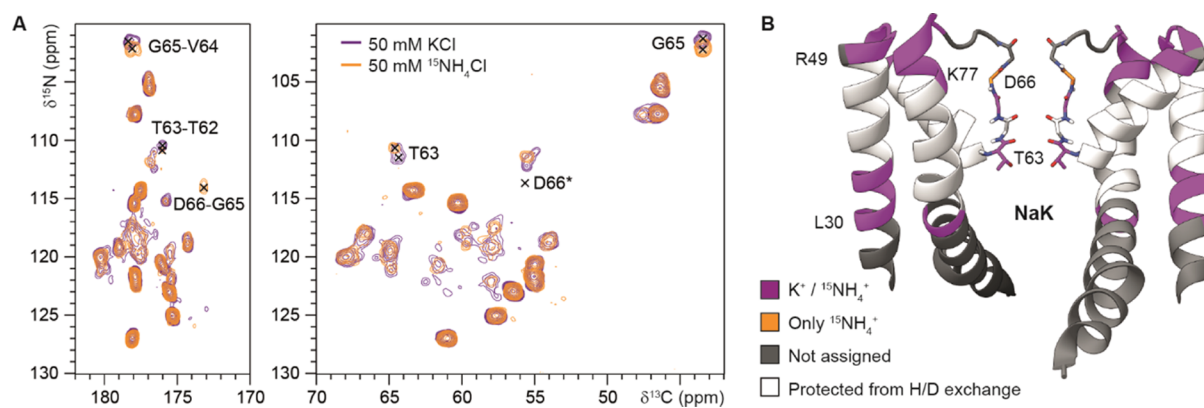


Figure 1. Comparison of K^+ and $^{15}\text{NH}_4^+$ -bound NaK. (A) Overlay of 2D NCO (left) and $\text{N}\alpha$ (right) projections from 3D (H)CONH and (H)CaNH spectra of NaK with 50 mM KCl (purple) or 50 mM $^{15}\text{NH}_4\text{Cl}$ (orange). *Note that in the $\text{N}\alpha$ projection, the peak corresponding to D66 is too weak to be visible; it could however be identified in the 3D hCaNH. (B) Assigned residues plotted onto the crystal structure of NaK (PDB ID 3E8H). Residues for which the amide protons are visible in H_2O back-exchanged $^{13}\text{C}^{15}\text{N}$ -labeled NaK (in both K^+ -bound and $^{15}\text{NH}_4^+$ -bound samples) are shown in purple. D66, which is only visible in $^{15}\text{NH}_4^+$ -bound NaK, is colored orange. Residues that could not be assigned (as previously)²⁵ are shown in dark grey, and residues that are protected from H/D exchange are shown in white.

BioSpin) on spectrometers operating at external magnetic field strengths corresponding to ^1H Larmor frequencies of 600 and 900 MHz (Bruker). The drift of the 600 MHz spectrometer is negligible, and therefore, no lock was needed. For experiments recorded on the 900 MHz spectrometer, an external lock was used. CP-based 2D (H)NH and 3D (H)CaNH experiments and 1D and/or 2D $^{15}\text{NH}_4^+$ -selective INEPT-based experiments were recorded for all deuterated samples (see Supporting Information Figure S1).

Additional CP-based 2D (H)CH, 3D (H)CONH, (H)CO(C α)-NH, and (H)Ca(CO)NH experiments were recorded for the samples where assignments were required for a complete analysis. A $^{15}\text{NH}_4^+$ -selective 3D H(H)NH experiment, with 25 ms ^1H - ^1H SD mixing, was recorded for deuterated NaK2K with 50 mM $^{15}\text{NH}_4\text{Cl}$. Assignment experiments [3D (H)CaNH, (H)CONH, (H)CO(C α)-NH, and (H)Ca(CO)NH] for the deuterated samples were recorded using 35% non-uniform sampling, with a sampling scheme generated from <http://gwagner.med.harvard.edu/intranet/hmsIST/>,^{27,28} reconstructed with the qMDD software using compressed sensing with the iterative re-weighted least squares algorithm^{29–31} (20 iterations) and processed using NMRPipe.³² Uniformly recorded spectra were processed using TopSpin 4 (Bruker). Spectral analysis was performed using CcpNmr Analysis.³³

The fully protonated $^{13}\text{C}, ^{15}\text{N}$ -KcsA-Kv1.3 sample in 50 mM KCl buffer was pre-packed in a 1.3 mm rotor and then transferred to a 0.7 mm rotor. Backbone assignment experiments, (H)CaNH, (H)(CO)-Ca(CO)NH, (H)CO(C α)NH, and (H)CONH, were measured on a 950 MHz Bruker spectrometer equipped with a 0.7 mm HCND probe with 105 kHz MAS with cooling gas set to 265 K. For the sample in 150 mM $^{15}\text{NH}_4\text{Cl}$ -containing buffer, (H)NH, (H)CaNH and (H)CONH spectra were measured using 100 kHz MAS on a 950 MHz Bruker spectrometer equipped with a 0.7 mm HCND probe with cooling gas set to 260 K. An (H)NH spectrum using a refocused INEPT transfer scheme to detect $^{15}\text{NH}_4^+$ was measured on a 1.2 GHz Bruker spectrometer using 100 kHz MAS at a 260 K set temperature.

MD Simulations. Molecular systems used for MD simulations of NaK2K F92A and KcsA were taken from our previous investigation.³⁴ For NaK2K F92A, a high-resolution crystal structure (PDB ID 3OUF) was used. For KcsA, the crystal structure (PDB ID 3F5W) was used, with the SF taken from another structure (PDB ID 1K4C). In NaK2K, the F92A mutation was introduced to increase ionic fluxes.⁴ Both channels were embedded in a patch of POPC lipids and surrounded by K^+ , Na^+ , and Cl^- ions. For simulations with ammonium ions, all K^+ ions were replaced by NH_4^+ ions. The final salt concentration was ca. 0.9 M. The titratable groups of channels were protonated according to their standard protonation states at pH 7 (in KcsA, E71 was protonated³⁵). The systems were simulated with GROMACS 5.1 or 2016^{36–39} under an electric field acting along the

z-axis (perpendicular to the membrane), resulting in a membrane voltage^{40,41} of 200 mV (for NaK2K F92A) or 300 mV (for KcsA) to drive outward ion permeation. 10 individual simulations were run for each channel/force field/ion combination (6 separate systems), each for 100–500 ns.

For NaK2K F92A simulations, two different force fields were used: Amber99sb⁴² and CHARMM36m.⁴³ For KcsA simulations, only Amber99sb was used, as the SF of KcsA shows instabilities in simulations with CHARMM36m.^{44,45} For Amber99sb simulations, Berger lipids,⁴⁶ the TIP3P water model,⁴⁷ and Joung and Cheatham K^+ and Cl^- ion parameters were used.⁴⁸ For NH_4^+ ions, default Amber99sb parameters were used. Aliphatic hydrogen atoms were treated with the virtual site technique, allowing for a 4 fs timestep.⁴⁹ van der Waals interactions were cut off at 1.0 nm, and the dispersion correction for energy and pressure was applied. The particle mesh Ewald (PME)⁵⁰ method was used for electrostatic interactions, with a 1.0 nm real-space cutoff. The v-rescale thermostat⁵¹ and semi-isotropic Berendsen barostat⁵² were used to keep the systems at 323 K and 1 bar, respectively. For CHARMM36m simulations, we used CHARMM36 lipids,⁵³ CHARMM TIP3P water model,⁵⁴ and default CHARMM ion parameters.⁵⁵ The integration time step was 2 fs. van der Waals interactions were force-switched off from 0.8 to 1.2 nm. The PME method was used with the 1.2 nm real-space cutoff. The Nosé-Hoover thermostat^{56,57} and Parrinello-Rahman barostat⁵⁸ were used to keep the systems at 320 K and 1 bar, respectively. For each system and force field, 10 individual simulations were run, each between 100–500 ns long. The analysis was done using a custom tool for K^+ channel simulations reported before.⁵⁹ A root-mean-square-deviation (RMSD) was calculated for SF mainchain atoms after fitting it to the high-resolution crystal structure (PDB ID 6UFE for NaK2K and PDB ID 5VK6 for KcsA) using the gmx rms tool.

RESULTS AND DISCUSSION

$^{15}\text{NH}_4^+$ Ions are Suitable as a Mimic for K^+ Ions in the Non-Selective Ion Channel NaK. A previous solid-state NMR study revealed that the SF of NaK can adopt two different conformations depending on the presence of K^+ or Na^+ ions in the sample. The K^+ -bound state corresponds to the conformation observed in the crystal structure (PDB ID 3E8H), while the Na^+ bound state is represented by a mixture between the crystal structure conformation and a conformation with a carbonyl flip of residue T62 just below the SF.²⁵ NaK is therefore an excellent system to evaluate whether $^{15}\text{NH}_4^+$ ions can be used as a K^+ mimic in solid-state NMR studies. The spectra can directly show clear differences depending on which

ions are bound. To address this, we recorded a set of ^1H -detected 3D spectra⁶⁰ on 100% H_2O back-exchanged deuterated $^{13}\text{C}^{15}\text{N}$ -labeled NaK samples with 50 mM $^{15}\text{NH}_4\text{Cl}$ or 50 mM KCl.

The only significant difference between the samples is that D66 can be detected in the $^{15}\text{NH}_4^+$ -bound sample but not in the K^+ -bound sample (see Figure 1 and Supporting Information Figure S2). This would suggest that $^{15}\text{NH}_4^+$ ions stabilize the upper part of the SF more than K^+ ions. Additionally, a small difference in the nitrogen chemical shift of G65 (0.8 ppm) can be observed, which could be related to the stabilization of the upper part of the SF caused by $^{15}\text{NH}_4^+$ ions and/or different chemical shielding between K^+ and $^{15}\text{NH}_4^+$ ions. However, since the CO atoms of the SF residues are closest to the ions and their chemical shifts are unaffected by the ion type present, it seems unlikely that different ions cause different chemical shielding. Finally, the nitrogen chemical shift of T63 appears to be slightly different between the two samples; however, this peak is rather weak and broad in both samples. The almost identical spectra for the two samples indicate that there are no significant structural differences between $^{15}\text{NH}_4^+$ -bound and K^+ -bound NaK, confirming that $^{15}\text{NH}_4^+$ is a good mimic for K^+ .

Bound $^{15}\text{NH}_4^+$ Ions Detected in the S3 and S4 Ion Binding Sites in NaK. To detect $^{15}\text{NH}_4^+$ ions, we used ^1H -detected (H)NH refocused INEPT experiments with INEPT delays specific to $^{15}\text{NH}_4^+$, assuming a J-coupling strength of 73.5 Hz⁶¹ (Supporting Information Figure S1). Bandwidth-selective pulses on the nitrogen channel can be used to filter out signals coming from the backbone and side-chain NH groups. This works well since the nitrogen chemical shifts of $^{15}\text{NH}_4^+$ ions are around 20–25 ppm, which is far away from any nitrogen chemical shifts originating from backbone or side-chain atoms (see Supporting Information Figure S3). It should be mentioned that at pH 8, which we have in our samples, free $^{15}\text{NH}_4^+$ ions in solution cannot be detected due to chemical exchange with bulk water. This is also obvious from the spectra, which otherwise would have contained an intense peak from free $^{15}\text{NH}_4^+$ ions. We are therefore able to specifically detect bound NH_4^+ ions within the SF of the non-selective ion channel.

The SF of NaK consists of two ion binding sites, S3 and S4 (see Figure 2A), and the $^{15}\text{NH}_4^+$ -selective ^1H -detected ^1H - ^{15}N 2D spectrum (Figure 2B) shows two peaks with different nitrogen chemical shifts (20.9 and 22.9 ppm). The $^{15}\text{NH}_4^+$ peak at 22.9 ppm appears to be split or broadened in the ^1H dimension. We used ^1H -detected ^1H - ^{13}C CP experiments with long mixing times (7–8 ms) to transfer magnetization between the protons of $^{15}\text{NH}_4^+$ ions and carbon atoms of NaK (Figure 2C right, orange spectrum). An ion bound in the S3 ion binding site should show transfer to T63 CO, V64 $\text{C}\alpha$, V64 CO, and G65 $\text{C}\alpha$. An ion bound in the S4 ion binding site should show transfer to T63 $\text{C}\alpha$, T63 $\text{C}\beta$, T63 $\text{C}\gamma$, T63 CO, and V64 CO. As a control, we performed the same experiments on NaK with K^+ ions (Figure 2C left, purple spectrum). Since the carbon chemical shifts are identical in K^+ - and $^{15}\text{NH}_4^+$ -bound NaK, we can easily identify cross-peaks between $^{15}\text{NH}_4^+$ ions and nearby carbon atoms of NaK. These cross-peaks will only be visible in the spectrum of $^{15}\text{NH}_4^+$ -bound NaK at the proton chemical shifts of the $^{15}\text{NH}_4^+$ ions (see Figure 2). All the cross-peaks corresponding to ions being bound in the S3 and S4 ion binding sites could be observed

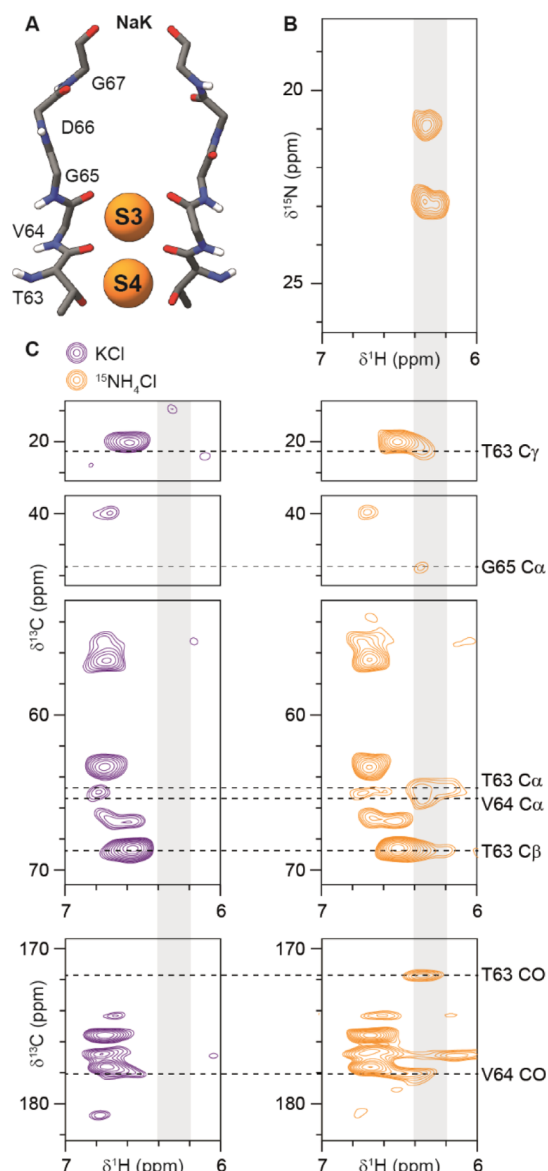


Figure 2. Detection of bound $^{15}\text{NH}_4^+$ ions in NaK. (A) SF structure of NaK, with the ion binding sites S3 and S4 indicated. (B) INEPT-based band-selective 2D ^1H - ^{15}N correlation spectrum of bound $^{15}\text{NH}_4^+$ ions. (C) ^1H -detected ^1H - ^{13}C correlation spectra (NaK with K^+ ions in purple and with $^{15}\text{NH}_4^+$ ions in orange) with 7–8 ms CP transfer times. The chemical shifts of carbon atoms in the SF residues T63, V64, and G65 are indicated with dashed lines, and the proton chemical shifts of the $^{15}\text{NH}_4^+$ ions are indicated with a gray shade. The spectra at the top were recorded with the carbon carrier frequency in the middle of the aliphatic region and the spectra at the bottom in the middle of the carbonyl region.

(Figure 2C). Unfortunately, the proton chemical shifts are not distinguishable between the two $^{15}\text{NH}_4^+$ peaks, and we therefore cannot unambiguously assign which peak belongs to which ion binding site. However, there appears to be a tail in the ^1H dimension on the $^{15}\text{NH}_4^+$ -T63 $\text{C}\alpha$ and $^{15}\text{NH}_4^+$ -T63 $\text{C}\beta$ cross-peaks. This implies that the $^{15}\text{NH}_4^+$ peak with a nitrogen chemical shift of 22.9 ppm and a split in the ^1H dimension could represent a slightly heterogeneous S4 ion binding site. The behavior of T63 N that appears as a broadened peak in our assignment experiments (Figure 1) also fits with a more dynamic S4 ion binding site. Overall, the experiments on NaK

show that $^{15}\text{NH}_4^+$ ions are a promising tool for solid-state NMR investigations of ion binding. We therefore applied these methods to the K^+ -selective mutant NaK2K (NaK D66Y and N68D) for which we previously used ^1H -detected solid-state NMR experiments to investigate the ion conduction mechanism by studying the behavior of water molecules.¹³

Bound $^{15}\text{NH}_4^+$ Ions in NaK2K Are Consistent with the Direct Knock-On Ion Conduction Mechanism. The K^+ -selective mutant NaK2K has the signature SF sequence TVGYG, which forms four ion binding sites (S1 to S4, see Figure 3A).³ In the same way as for NaK, we recorded ^1H - ^{15}N correlation spectra of $^{15}\text{NH}_4^+$ ions in 100% H_2O back-

exchanged deuterated $^{13}\text{C}^{15}\text{N}$ -labeled protein using INEPT-based transfers. In contrast to NaK, for which two $^{15}\text{NH}_4^+$ peaks were detected (Figure 2B), four $^{15}\text{NH}_4^+$ peaks were detected in NaK2K (Figure 3B). The four ions detected in the SF of NaK2K provide an excellent opportunity to investigate the ion conduction mechanism. In the water-mediated ion conduction mechanism, alternating ions and water molecules should be present in the SF, whereas in the direct knock-on mechanism, predominantly ions should be present in the SF.

To investigate whether any of the ions are in close proximity to bound water molecules, we recorded a $^{15}\text{NH}_4^+$ -selective 3D H(H)NH experiment, with 25 ms ^1H - ^1H SD mixing. Any $^{15}\text{NH}_4^+$ ions that are in close proximity to bound water should give a peak in the SD spectrum. The fact that only one out of the four peaks gives a cross-peak with water is in strong agreement with the direct knock-on ion conduction mechanism and our previous results on K^+ -bound NaK2K.^{10,13}

Assignments of the $^{15}\text{NH}_4^+$ peaks were achieved using ^1H - ^{13}C CP experiments with long transfer times (8 ms, see Figure 3C) in the same way as described above for NaK. Since only one of the $^{15}\text{NH}_4^+$ peaks is in close proximity to water, it must come from a $^{15}\text{NH}_4^+$ ion bound in the S1 or S4 ion binding site. The $^{15}\text{NH}_4^+$ peak with a ^{15}N chemical shift of 19.7 ppm and a ^1H chemical shift of 6.35 ppm could be assigned to an ion bound in S4 based on transfers to T63 $\text{C}\alpha$, $\text{C}\beta$, $\text{C}\gamma$, and CO , meaning that the peak that is in close proximity to bound water must come from an ion bound in S1. This is also in agreement with a recent study where it was shown by crystallography and MD simulations that NaK2K has a hydrophobic gate below the SF that drastically limits the availability of water below the SF (near the S4 ion binding site).⁵ We could assign the peak with a ^{15}N chemical shift of 23.2 ppm (which has the same ^1H chemical shift as S1) to an ion bound in S3 based on transfers to T63 CO , T64 CO , and V64 $\text{C}\alpha$. Note that the S3-V64 $\text{C}\alpha$ cross-peak (labeled with * in Figure 2C) could not be unambiguously assigned since it overlaps with cross-peaks that are also present in the K^+ -bound sample. The additional cross-peaks in this region correspond to D52H-P50 $\text{C}\alpha$ and T80H γ 1 (the proton in the side-chain OH group of threonine)- $\text{C}\alpha$ (see Figure 3C, left spectrum). The last $^{15}\text{NH}_4^+$ peak was tentatively assigned to the remaining S2 ion binding site. Unfortunately, the SF residues G65 and Y66 do not show up in spectra of NaK2K with $^{15}\text{NH}_4^+$, and we could therefore not confirm the assignments of S1 and S2 using ^1H - ^{13}C correlation experiments. Consequently, it cannot be excluded that the peak tentatively assigned to S2 is a second conformation of one of the other ion binding sites.

Effects of $^{15}\text{NH}_4^+$ Ions Compared to K^+ Ions on the K^+ -Selective Mutant NaK2K. While NaK remained mostly unaffected by the binding of $^{15}\text{NH}_4^+$ ions compared to the binding of K^+ ions (Figure 1), spectra of NaK2K exhibited several differences (see Supporting Information Figure S4). Not only did we observe two conformations for several residues but also noted a different H/D exchange pattern when we exchanged the ions in the sample depending on which ions ($^{15}\text{NH}_4^+$ or K^+) were initially present in the sample (see Supporting Information Figure S5). So far, all experiments presented in this article have been performed on 100% H_2O back-exchanged deuterated $^{13}\text{C}^{15}\text{N}$ -labeled protein, meaning that only back-exchanged protons are visible in the spectra.

For a more detailed analysis of the effects of $^{15}\text{NH}_4^+$ binding in NaK2K, we prepared a fully protonated $^{13}\text{C}^{15}\text{N}$ -labeled sample (see Supporting Information Figure S6 for ^{13}C detected

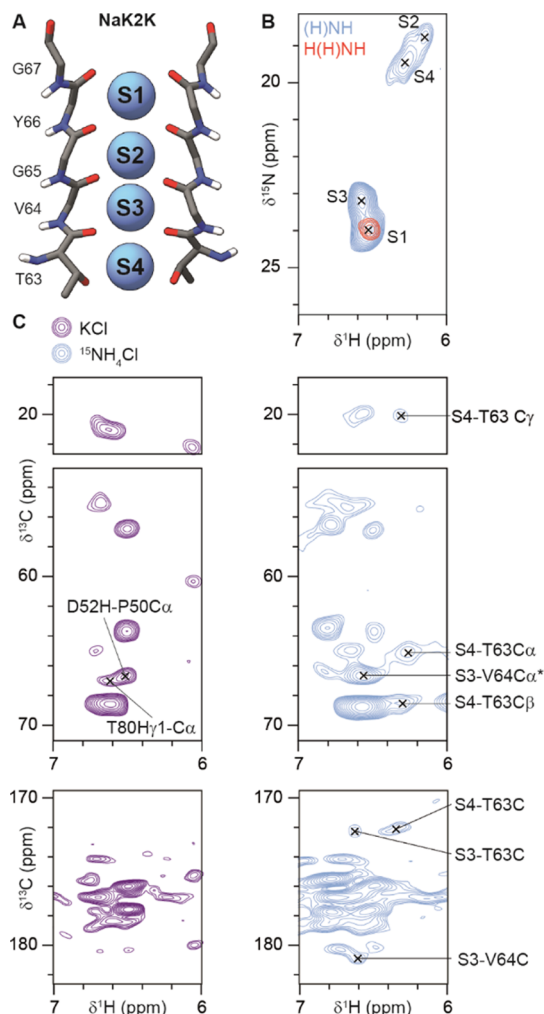


Figure 3. Detection of bound $^{15}\text{NH}_4^+$ ions in NaK2K. (A) SF structure of NaK2K, with the ion binding sites S1 to S4 indicated. (B) INEPT-based band-selective 2D ^1H - ^{15}N correlation spectrum of bound $^{15}\text{NH}_4^+$ ions (blue) overlaid with a 2D plane of a 3D H(H)NH experiment with a 25 ms ^1H - ^1H spin-diffusion mixing time taken at the chemical shift of bound water (red). (C) ^1H -detected ^1H - ^{13}C correlation spectra (NaK2K with K^+ in purple and with $^{15}\text{NH}_4^+$ in blue) with 8 ms CP transfer times. The identified cross-peaks between bound $^{15}\text{NH}_4^+$ ions and backbone atoms of NaK2K are labeled in the spectra of $^{15}\text{NH}_4^+$ -bound NaK2K. *Note that the cross-peak between S3 and V64 $\text{C}\alpha$ could not be unambiguously assigned due to potential overlaps with D52H-P50 $\text{C}\alpha$ and/or T80H γ 1- $\text{C}\alpha$ (labeled in the spectrum of K^+ -bound NaK2K). The spectra at the top were recorded with the carbon carrier frequency in the middle of the aliphatic region and the spectra at the bottom in the middle of the carbonyl region.

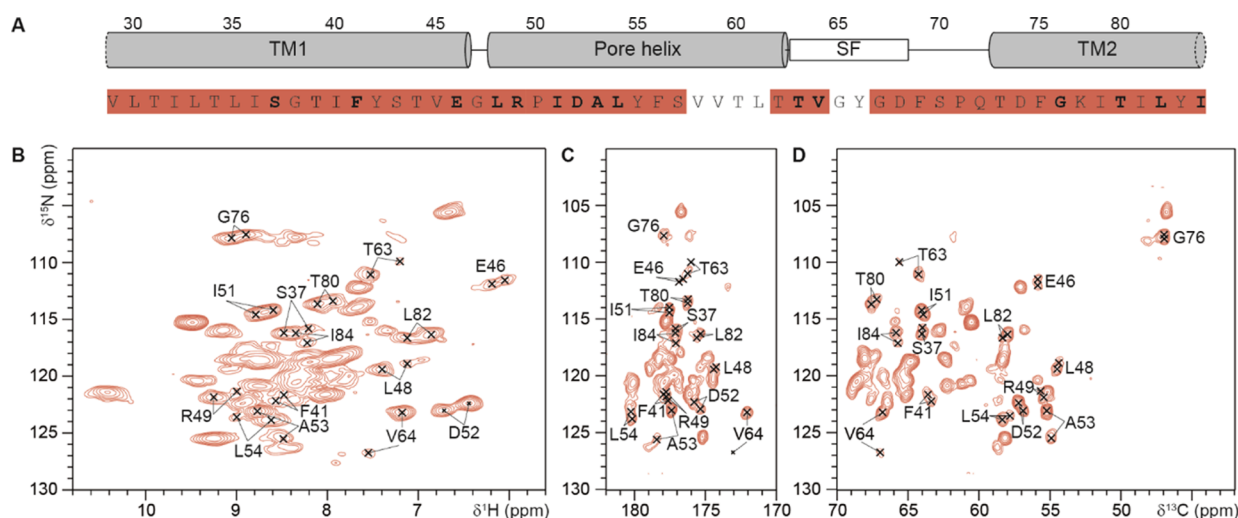


Figure 4. Assignments and multiple conformations of $^{15}\text{NH}_4^+$ -bound NaK2K. (A) Amino acid sequence of the assigned region of NaK2K with assigned residues indicated in red and residues for which two conformations could be identified indicated in bold letters. (B) 2D NH projection of a 3D (H) $\text{C}\alpha\text{NH}$, (C) 2D NCO projection of a 3D (H)CONH, and (D) 2D NC α projection of a 3D (H) $\text{C}\alpha\text{NH}$ recorded on fully protonated $^{13}\text{C}^{15}\text{N}$ -labeled NaK2K with 50 mM $^{15}\text{NH}_4\text{Cl}$. All residues showing two clear conformations are indicated in the spectra. In the NH and NC α projections, both chemical shifts for each peak correspond to the indicated residue, while in the NCO projection, the ^{15}N chemical shift corresponds to the indicated residue and the ^{13}C chemical shift to the preceding residue. Note that residues 58–61 could not be unambiguously assigned due to severe peak overlaps, and residues 65–67 are not present in the spectra.

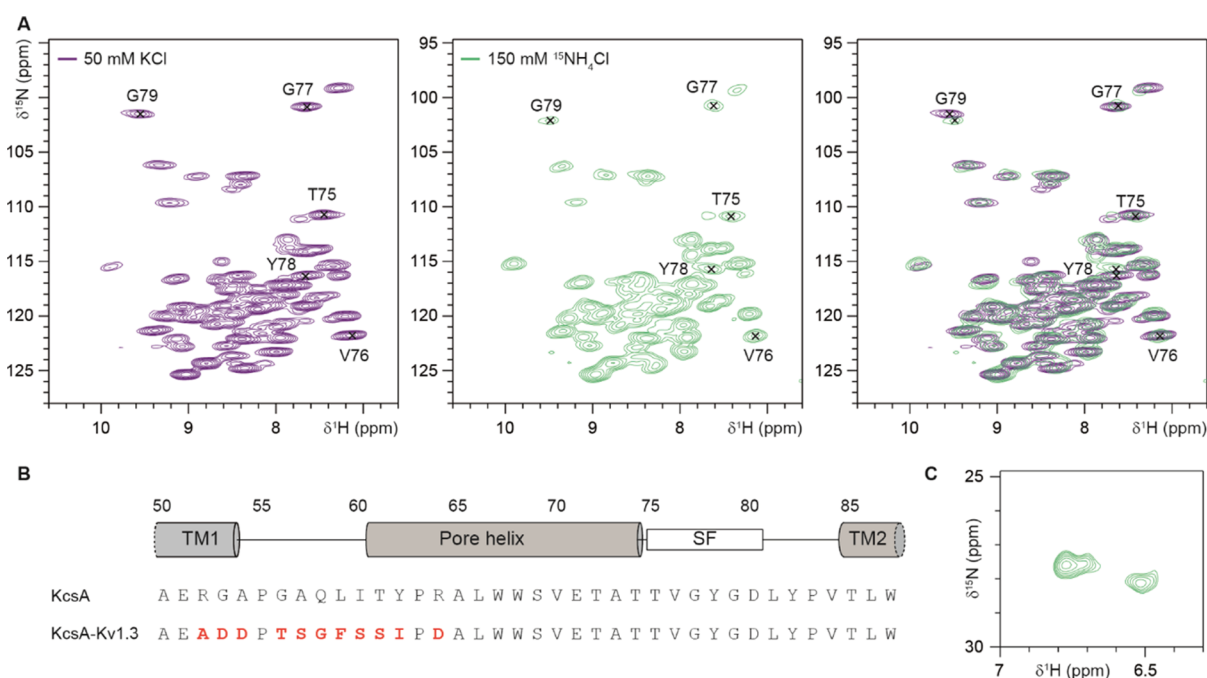


Figure 5. $^{15}\text{NH}_4^+$ binding in KcsA-Kv1.3. (A) 2D NH projections from 3D (H) $\text{C}\alpha\text{NH}$ spectra of KcsA-Kv1.3 with 50 mM KCl (left, purple), 150 mM $^{15}\text{NH}_4\text{Cl}$ (middle, green), and both spectra overlaid (right). The SF residues are indicated in the spectra. (B) Amino acid sequence of KcsA-Kv1.3 compared to KcsA, with mutations indicated in red. (C) 2D (H)NH spectrum of bound $^{15}\text{NH}_4^+$ ions.

spectra). In order to achieve high-quality ^1H -detected spectra, we performed the experiments at 100 kHz MAS (Figure 4). The presence of two peaks for several residues in $^{15}\text{NH}_4^+$ -bound NaK2K complicated the assignment process, and the lower part of the pore helix (V58–L61) could not be unambiguously assigned. The SF residues G65 and Y66 were not visible in the spectra.

The residues that show two distinct peaks are located in the lower part of the SF (T63 and V64), in the upper part of the pore helix (R49, I51, D52, A53, and L54), and on the

interacting parts of TM1 (S37 and F41) and TM2 (G76, T80, L82, and I84). First, it should be mentioned that one of the two assignments for any residue that has two conformations always fits with the single conformation observed for that residue in the K^+ -bound sample. The only exception is the CO resonance of V64, where only one conformation is visible in the $^{15}\text{NH}_4^+$ -bound sample, and this differs from the K^+ -bound sample by 1.1 ppm. Second, the chemical shift differences between the two observed conformations are almost exclusively noticeable for ^1H and ^{15}N chemical shifts (see

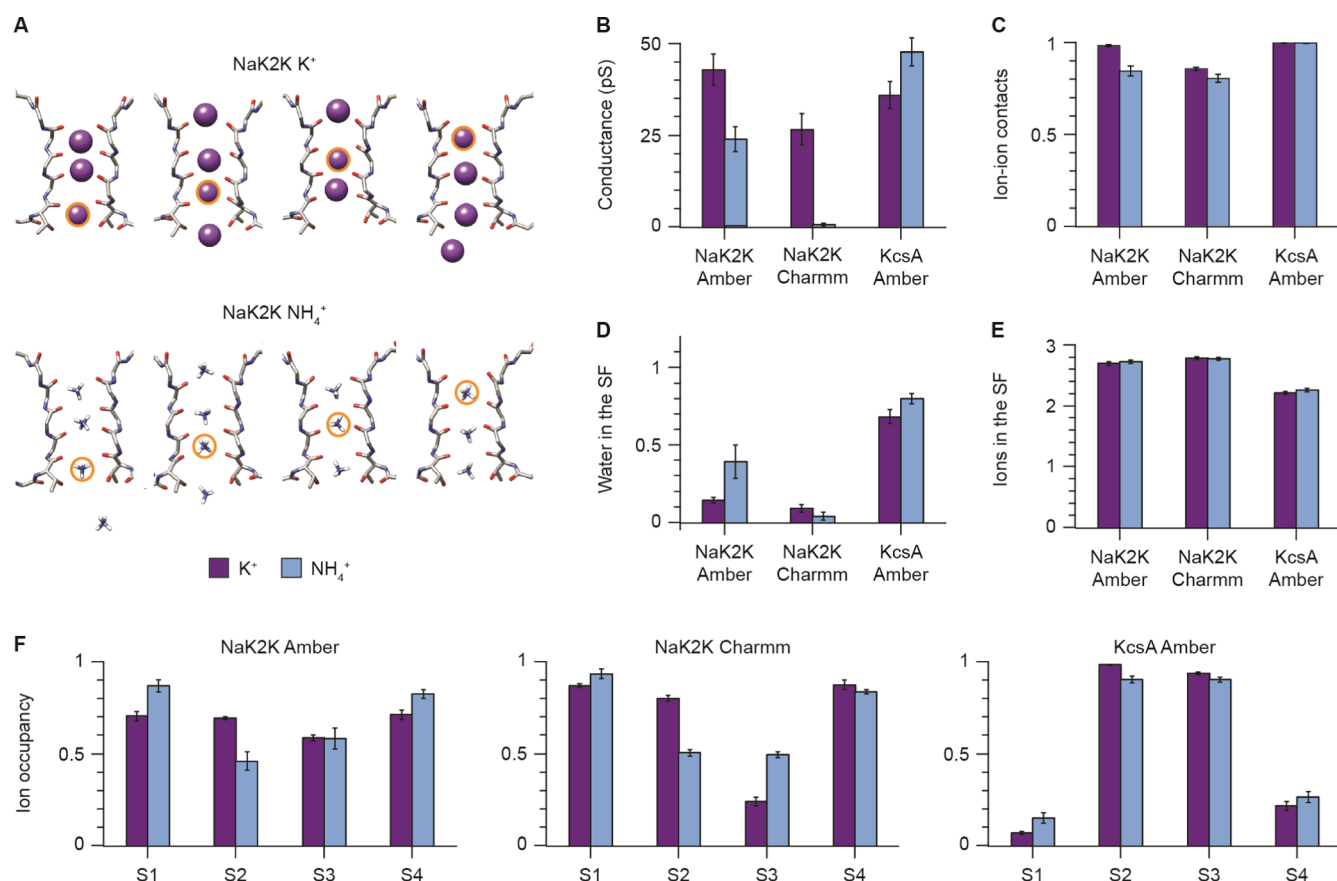


Figure 6. MD simulations of NaK2K F92A and KcsA with K⁺ and NH₄⁺ ions. (A) Snapshots from the simulations of NaK2K F92A with K⁺ (top) and NH₄⁺ (bottom). Orange circles represent an ion moving from the S4 to the S1 ion binding site. (B) Average conductance. (C) Average fraction of ion–ion contacts in the SF. (D) Average number of water molecules in the SF. (E) Average number of ions in the SF. (F) Average ion occupancy for each of the ion binding sites. All the plots (B–F) contain averages of 8–10 simulations, and the error bars represent the standard error of the mean. Simulations with K⁺ ions are represented by purple bars, and simulations with NH₄⁺ ions are represented by blue bars.

Figure 4B–D). This indicates that ¹⁵NH₄⁺ binding does not cause any significant effect on the overall structure of NaK2K, but the effect seems to be a change in the interactions between residues. The only ¹³C resonances that show chemical shift differences above 1 ppm between the two conformations are D52 CO, T63 CO, and T63 C α . The two conformations of I51 CO have a chemical shift difference of 0.4 ppm. All others are around 0.2 ppm or smaller, which is around the expected error in the assignments of ¹³C chemical shifts in these samples (see Supporting Information Tables S1 and S2). We previously described that in the absence of K⁺ ions and in the presence of Na⁺ ions, the SF of NaK2K is not stabilized.⁶² The residues affected by ¹⁵NH₄⁺ ions are in the same region of the protein as the residues affected by Na⁺ ions. Interestingly, the second conformation of the peaks that show two conformations in the presence of ¹⁵NH₄⁺ matches with the peaks that are shifted, compared to a K⁺-bound sample, in the presence of Na⁺ (see Supporting Information Figure S6 and Tables S1 and S2). This would suggest that the ¹⁵NH₄⁺-bound sample is in a state of mixed conformations between the K⁺-stabilized conformation and the conformation with an unstable SF that we previously observed in the presence of Na⁺ ions.

¹⁵NH₄⁺ Ions Work Well as a Mimic for K⁺ Ions in KcsA-Kv1.3. Based on the NaK2K data, we cannot determine whether ¹⁵NH₄⁺ ions should be considered as a good mimic for K⁺ in K⁺-selective ion channels. Therefore, we chose to also investigate the K⁺-selective ion channel KcsA-Kv1.3 (see

Supporting Information Figure S7 for SF assignments), which is a mutant of KcsA that is used as a model system for the pore domain of the human voltage-gated ion channel Kv1.3^{24,63} (Figure 5B shows which residues are mutated). KcsA-Kv1.3 can, in the same way as KcsA, adopt a conductive or non-conductive SF state depending on the pH and K⁺ concentration.^{64,65} This provides a good opportunity to test whether ¹⁵NH₄⁺ ions interact in the same way as K⁺ ions. Interestingly, KcsA-Kv1.3 does not behave as NaK2K when K⁺ ions are replaced by ¹⁵NH₄⁺ ions, but instead, we see a similar behavior as in NaK. The chemical shifts are almost identical between ¹⁵NH₄⁺- and K⁺-bound KcsA-Kv1.3 samples (Figure 5A). A few small chemical shift differences can be observed for some of the SF residues, the largest being the nitrogen chemical shifts of Y78 and G79 (0.6 ppm). There are no significant chemical shift differences for ¹³C atoms, the largest being 0.4 ppm for the ¹³CO of Y78, and there is no peak splitting (see also Supporting Information Figure S8 and Table S3). The 2D (H)NH refocused INEPT spectrum (with ¹⁵NH₄⁺ optimized delays) shows two peaks with different ¹⁵N chemical shifts in the ¹⁵NH₄⁺ region, with one of them showing a split in the ¹H dimension (Figure 5C). This could represent two or three ions bound in the SF of KcsA-Kv1.3 under equilibrium conditions (i.e., without voltage). The chemical shifts of the ¹⁵NH₄⁺ peaks are remarkably different from what we observed in NaK and NaK2K, indicating that ion binding can be significantly different between different ion

channels even if the SF sequences are identical. It should be mentioned that these experiments were performed on a sample that was previously in the presence of 50 mM KCl and later washed to 150 mM $^{15}\text{NH}_4\text{Cl}$.

Molecular Dynamics Simulations Show High Similarities between NH_4^+ and K^+ Ions. To further evaluate our approach, we conducted MD simulations under an applied electric field on NaK2K F92A and KcsA. Conduction of ions could be observed both with K^+ and NH_4^+ ions for both proteins (see Figure 6A,B and Movie S1).

The structures of the ion channels were generally stable during the simulations (see Supporting Information Figure S9 for RMSD plots of the SF mainchain atoms). However, in one simulation of NaK2K F92A and in two simulations of KcsA (all with NH_4^+ ions and the AMBER force field), we observed a rearrangement of the interactions between the SF and the pore helix, leading to unstable and more dynamic SF conformations. The most pronounced conformational changes in the deviating simulations are the loss of hydrogen bonds between the SF and the pore helix (D68–Y55 in NaK2K F92A, D80–W67 and E71 in KcsA). These unstable simulations were excluded from the analysis in Figure 6 (see Supporting Information Figures S10 and S11 and Tables S4 and S5 for a comparison between stable and unstable simulations).

Overall, the behavior of K^+ and NH_4^+ ions is very similar in the stable MD simulations. For NaK2K F92A, in the Amber force field, the conductance appears to be slightly lower with NH_4^+ compared to K^+ ions, but for KcsA, the conductance is very similar with the different ions (Figure 6B). The simulations of NaK2K F92A with NH_4^+ ions using the Charmm force field resulted in very low conductance, which can be explained by ions being stuck oscillating between two states (Supporting Information Figure S12). Therefore, an ion leaving the SF is a rare event. There is generally a slightly lower number of ion–ion contacts (Figure 6C) and a larger number of water molecules in the SF (Figure 6D) in the simulations with NH_4^+ ions, whereas the number of ions in the SF (Figure 6E) is not affected, showing that water molecules do not take part in ion conduction. The preference for the different ion binding sites is slightly different between K^+ and NH_4^+ ions, though. The most pronounced differences are observed in simulations of NaK2K F92A using the Charmm force field where S2 and S3 are equally occupied when NH_4^+ ions are used, but S2 has a much higher occupancy than S3 when K^+ ions are used (Figure 6F). The most interesting observation regarding occupancy is however the differences between NaK2K F92A and KcsA. NaK2K F92A shows a relatively small variation in occupancy between the ion binding sites (with the exception of S3 in the simulations with K^+ and the Charmm force field) with a slight preference for the S1 and S4 ion binding sites, while in KcsA, the S2 and S3 ion binding sites are almost always occupied, but the S1 and S4 ion binding sites show low occupancy. This agrees well with the different $^{15}\text{NH}_4^+$ solid-state NMR spectra for NaK2K (Figure 3B) and KcsA-Kv1.3 (Figure 5C).

During the simulations of NH_4^+ conduction, the ions appear to rotate quickly so that the protons sample all different orientations compared to the nitrogen atom (Movie S1). Such a rotation leads to efficient averaging of ^1H – ^{15}N dipolar couplings in solid-state NMR experiments and can explain why dipolar-based magnetization transfer between the ^1H and ^{15}N atoms in the $^{15}\text{NH}_4^+$ ions was not possible.

Apart from the observed agreement, two setup differences between MD and solid-state NMR are expected to result in qualitative differences, in particular regarding water molecules in the channel. First, the MD simulations of NaK2K were based on the F92A mutant, whereas the solid-state NMR experiments did not include this mutation. Second, an external electric field was applied in the simulations but was absent in the experiments. The F92A mutant ensures conductance and therefore convergence of the filter occupancies on the short MD timescales. Such free access, especially for water, might be restricted in the solid-state NMR experiments based on wild-type NaK2K.⁵ Consequently, even though water molecules do not permeate the channels, they transiently occupy S4 ion binding sites during conduction in MD simulations (Movie S1), which is not observed in solid-state NMR. Likewise, the applied electric field in the MD simulations leads to a further enhancement of water occupancy in the filter due to stabilization of the water dipoles by aligning with the applied field. We assume that these two effects result in higher water occupancy in the SF in the MD simulations as compared to the solid-state NMR experiments.

CONCLUSIONS

We have shown, for the first time, direct detection of ions bound in the SF of ion channels under native-like conditions, i.e. embedded in liposomes at room temperature using physiological buffer conditions. Magnetization transfer between $^{15}\text{NH}_4^+$ ions and water in NaK2K showed that only one of the four ions (the one in binding site S1) is in close proximity to bound water, adding to the experimental evidence for the direct knock-on ion conduction mechanism¹⁰ for K^+ -selective ion channels.

While $^{15}\text{NH}_4^+$ ions worked perfectly as a mimic for K^+ ions in the non-selective ion channel NaK, there were some spectral differences between $^{15}\text{NH}_4^+$ and K^+ -bound NaK2K. In the presence of $^{15}\text{NH}_4^+$ ions, NaK2K adopts a mixed conformation between a K^+ -stabilized and a destabilized state. The chemical shifts of the destabilized state fit remarkably well with the chemical shifts of NaK2K in the presence of Na^+ ions.⁶² In contrast, experiments on KcsA-Kv1.3 showed that $^{15}\text{NH}_4^+$ ions did not have any destabilizing effects on this channel and that the behavior we observed in NaK2K is not general for K^+ -selective ion channels. The destabilized state in NaK2K might be related to a loss of the stabilizing hydrogen bond between D68 above the SF and Y55 in the pore helix. In MD simulations of both NaK2K F92A and KcsA, a loss of stabilizing hydrogen bonds between the SF and the pore helix resulted in a destabilized SF. In this state, we observed an increase in water in the ion binding sites and no or very low conduction (Supporting Information Figures S10 and S11, Tables S4 and S5). In KcsA, the stabilizing hydrogen bond contains residue E71 in the pore helix. Mutations of E71 have previously been shown to affect the conformational dynamics of the SF in KcsA.^{17,66} The different patterns of $^{15}\text{NH}_4^+$ peaks in different ion channels suggest that ion binding is not identical in all K^+ -selective ion channels even though the sequences and crystal structures of the SFs may be highly similar. Interestingly, the MD simulations also showed a distinctly different behavior between NaK2K F92A and KcsA in regards to which ion binding sites are most occupied during ion conduction. While in NaK2K F92A the occupancy of the different ion binding sites appears to be more evenly distributed, there is a strong preference for the S2 and S3

ion binding sites in KcsA. This agrees well with the solid-state NMR experiments of bound ammonium ions (4 peaks in NaK2K, 2–3 peaks in KcsA-Kv1.3).

Solid-state NMR experiments using $^{15}\text{NH}_4^+$ ions as a mimic of K^+ ions can be a useful tool for future characterization of ion binding in SFs and aid in the understanding of ion conduction and gating mechanisms in ion channels.

■ ASSOCIATED CONTENT

SI Supporting Information

The Supporting Information is available free of charge at <https://pubs.acs.org/doi/10.1021/jacs.1c13247>.

Scheme of pulse program used for detection of $^{15}\text{NH}_4^+$ ions, comparison of 2D NCO and $\text{NC}\alpha$ projections between K^+ - and $^{15}\text{NH}_4^+$ -bound NaK, spectra of $^{15}\text{NH}_4^+$ ions with and without selective pulses, comparison of (H)NH spectra between K^+ - and $^{15}\text{NH}_4^+$ -bound NaK2K, H/D exchange pattern and effects of changing the ions in NaK2K, comparison of $\text{NC}\alpha$ and NCO spectra between K^+ , $^{15}\text{NH}_4^+$ - and Na^+ -bound NaK2K, backbone walk for the SF of KcsA-Kv1.3, comparison of 2D NCO and $\text{NC}\alpha$ projections between K^+ - and $^{15}\text{NH}_4^+$ -bound KcsA-Kv1.3, plots showing RMSDs for SF mainchain atoms compared to the starting structures during MD simulations, comparison between stable and unstable SF conformations based on MD simulations for NaK2K F92A and KcsA, main states for NaK2K F92A in simulations with NH_4^+ ions using the Charmm force field, assigned chemical shifts, and data extracted from MD simulations, movie showing NH_4^+ ion conduction (PDF) (MPG)

■ AUTHOR INFORMATION

Corresponding Author

Adam Lange – Department of Molecular Biophysics, Leibniz-Forschungsinstitut für Molekulare Pharmakologie, 13125 Berlin, Germany; Institut für Biologie, Humboldt-Universität zu Berlin, 10115 Berlin, Germany; orcid.org/0000-0002-7534-5973; Email: alange@fmp-berlin.de

Authors

Carl Öster – Department of Molecular Biophysics, Leibniz-Forschungsinstitut für Molekulare Pharmakologie, 13125 Berlin, Germany; orcid.org/0000-0002-8723-4533
Kumar Tekwani Movellan – Department of NMR-Based Structural Biology, Max Planck Institute for Multidisciplinary Sciences, 37077 Göttingen, Germany
Benjamin Goold – Faculty of Engineering and Physical Sciences, University of Southampton, SO17 1BJ Southampton, U.K.; Computational Biomolecular Dynamics Group, Max Planck Institute for Multidisciplinary Sciences, 37077 Göttingen, Germany
Kitty Hendriks – Department of Molecular Biophysics, Leibniz-Forschungsinstitut für Molekulare Pharmakologie, 13125 Berlin, Germany
Sascha Lange – Department of Molecular Biophysics, Leibniz-Forschungsinstitut für Molekulare Pharmakologie, 13125 Berlin, Germany
Stefan Becker – Department of NMR-Based Structural Biology, Max Planck Institute for Multidisciplinary Sciences, 37077 Göttingen, Germany

Bert L. de Groot – Computational Biomolecular Dynamics Group, Max Planck Institute for Multidisciplinary Sciences, 37077 Göttingen, Germany; orcid.org/0000-0003-3570-3534

Wojciech Kopec – Computational Biomolecular Dynamics Group, Max Planck Institute for Multidisciplinary Sciences, 37077 Göttingen, Germany; orcid.org/0000-0001-8801-9563

Loren B. Andreas – Department of NMR-Based Structural Biology, Max Planck Institute for Multidisciplinary Sciences, 37077 Göttingen, Germany; orcid.org/0000-0003-3216-9065

Complete contact information is available at:

<https://pubs.acs.org/doi/10.1021/jacs.1c13247>

Author Contributions

The article was written through contributions of all authors.

Notes

The authors declare no competing financial interest.

■ ACKNOWLEDGMENTS

We thank Dagmar Michl and Karin Giller for expert technical assistance. This work was funded by the Leibniz-Forschungsinstitut für Molekulare Pharmakologie (FMP) and the Deutsche Forschungsgemeinschaft (DFG, German Research Foundation) under Germany's Excellence Strategy—EXC 2008—390540038—UniSysCat. C.Ö. acknowledges funding from the Human Frontier Science Program LT000303-2019-L. W.K. and B.L.d.G. acknowledge funding from the German Research Foundation DFG through FOR 2518, project P5. S.B. is supported by the Max Planck Society. L.B.A. acknowledges funding from the DFG Emmy Noether program (grant AN1316).

■ REFERENCES

- (1) Hille, B. *Ionic Channels of Excitable Membranes*, 3rd ed.; Sinauer: Sunderland, MA, 2001; pp 131–168.
- (2) Shi, N.; Ye, S.; Alam, A.; Chen, L.; Jiang, Y. Atomic Structure of a Na^+ - and K^+ -Conducting Channel. *Nature* **2006**, *440*, 570–574.
- (3) Derebe, M. G.; Sauer, D. B.; Zeng, W.; Alam, A.; Shi, N.; Jiang, Y. Tuning the Ion Selectivity of Tetrameric Cation Channels by Changing the Number of Ion Binding Sites. *Proc. Natl. Acad. Sci. U.S.A.* **2011**, *108*, 598–602.
- (4) Sauer, D. B.; Zeng, W.; Cauty, J.; Lam, Y.; Jiang, Y. Sodium and Potassium Competition in Potassium-Selective and Non-Selective Channels. *Nat. Commun.* **2013**, *4*, 2721.
- (5) Langan, P. S.; Vandavasi, V. G.; Kopec, W.; Sullivan, B.; Afonine, P. V.; Weiss, K. L.; de Groot, B. L.; Coates, L. The Structure of a Potassium-Selective Ion Channel Reveals a Hydrophobic Gate Regulating Ion Permeation. *IUCrJ* **2020**, *7*, 835–843.
- (6) Doyle, D. A.; Cabral, J. M.; Pfuetzner, R. A.; Kuo, A.; Gulbis, J. M.; Cohen, S. L.; Chait, B. T.; MacKinnon, R. The Structure of the Potassium Channel: Molecular Basis of K^+ Conduction and Selectivity. *Science* **1998**, *280*, 69–77.
- (7) Coates, L. Ion Permeation in Potassium Ion Channels. *Acta Crystallogr., Sect. D: Struct. Biol.* **2020**, *76*, 326–331.
- (8) Mironenko, A.; Zachariae, U.; de Groot, B. L.; Kopec, W. The Persistent Question of Potassium Channel Permeation Mechanisms. *J. Mol. Biol.* **2021**, *433*, 167002.
- (9) Morais-Cabral, J. H.; Zhou, Y.; MacKinnon, R. Energetic Optimization of Ion Conduction Rate by the K^+ Selectivity Filter. *Nature* **2001**, *414*, 37–42.
- (10) Köpfer, D. A.; Song, C.; Gruene, T.; Sheldrick, G. M.; Zachariae, U.; de Groot, B. L. Ion Permeation in K^+ Channels Occurs by Direct Coulomb Knock-On. *Science* **2014**, *346*, 352–355.

- (11) Kratochvil, H. T.; Carr, J. K.; Matulef, K.; Annen, A. W.; Li, H.; Maj, M.; Ostmeier, J.; Serrano, A. L.; Raghuraman, H.; Moran, S. D.; Skinner, J. L.; Perozo, E.; Roux, B.; Valiyaveetil, F. I.; Zanni, M. T. Instantaneous Ion Configurations in the K⁺ Ion Channel Selectivity Filter Revealed by 2D IR Spectroscopy. *Science* **2016**, *353*, 1040–1044.
- (12) Langan, P. S.; Vandavasi, V. G.; Weiss, K. L.; Afonine, P. V.; el Omari, K.; Duman, R.; Wagner, A.; Coates, L. Anomalous X-Ray Diffraction Studies of Ion Transport in K⁺ Channels. *Nat. Commun.* **2018**, *9*, 4540.
- (13) Öster, C.; Hendriks, K.; Kopec, W.; Chevelkov, V.; Shi, C.; Michl, D.; Lange, S.; Sun, H.; de Groot, B. L.; Lange, A. The Conduction Pathway of Potassium Channels Is Water Free under Physiological Conditions. *Sci. Adv.* **2019**, *5*, No. eaaw6756.
- (14) Hud, N. V.; Schultze, P.; Feigon, J. Ammonium Ion as an NMR Probe for Monovalent Cation Coordination Sites of DNA Quadruplexes. *J. Am. Chem. Soc.* **1998**, *120*, 6403–6404.
- (15) Werbeck, N. D.; Kirkpatrick, J.; Reinstein, J.; Hansen, D. F. Using 15 N-Ammonium to Characterise and Map Potassium Binding Sites in Proteins by NMR Spectroscopy. *ChemBioChem* **2014**, *15*, 543–548.
- (16) Eichmann, C.; Frey, L.; Maslennikov, I.; Riek, R. Probing Ion Binding in the Selectivity Filter of the KcsA Potassium Channel. *J. Am. Chem. Soc.* **2019**, *141*, 7391–7398.
- (17) Jekhmane, S.; Medeiros-Silva, J.; Li, J.; Kümmerer, F.; Müller-Hermes, C.; Baldus, M.; Roux, B.; Weingarth, M. Shifts in the Selectivity Filter Dynamics Cause Modal Gating in K⁺ Channels. *Nat. Commun.* **2019**, *10*, 123.
- (18) Shcherbakov, A. A.; Hisao, G.; Mandala, V. S.; Thomas, N. E.; Soltani, M.; Salter, E. A.; Davis, J. H.; Henzler-Wildman, K. A.; Hong, M. Structure and Dynamics of the Drug-Bound Bacterial Transporter EmrE in Lipid Bilayers. *Nat. Commun.* **2021**, *12*, 172.
- (19) Shi, C.; Öster, C.; Bohg, C.; Li, L.; Lange, S.; Chevelkov, V.; Lange, A. Structure and Dynamics of the Rhomboid Protease GlpG in Liposomes Studied by Solid-State NMR. *J. Am. Chem. Soc.* **2019**, *141*, 17314–17321.
- (20) Joedicke, L.; Mao, J.; Kuenze, G.; Reinhart, C.; Kalavacherla, T.; Jonker, H. R. A.; Richter, C.; Schwalbe, H.; Meiler, J.; Preu, J.; Michel, H.; Glaubitz, C. The Molecular Basis of Subtype Selectivity of Human Kinin G-Protein-Coupled Receptors. *Nat. Chem. Biol.* **2018**, *14*, 284–290.
- (21) Schubeis, T.; Le Marchand, T.; Daday, C.; Kopec, W.; Tekwani Movellan, K.; Stanek, J.; Schwarzer, T. S.; Castiglione, K.; de Groot, B. L.; Pintacuda, G.; Andreas, L. B. A β -Barrel for Oil Transport through Lipid Membranes: Dynamic NMR Structures of AlkL. *Proc. Natl. Acad. Sci. U.S.A.* **2020**, *117*, 21014–21021.
- (22) Medeiros-Silva, J.; Mance, D.; Daniëls, M.; Jekhmane, S.; Houben, K.; Baldus, M.; Weingarth, M. 1 H-Detected Solid-State NMR Studies of Water-Inaccessible Proteins In Vitro and In Situ. *Angew. Chem., Int. Ed.* **2016**, *55*, 13606–13610.
- (23) Good, D.; Pham, C.; Jagas, J.; Lewandowski, J. R.; Ladizhansky, V. Solid-State NMR Provides Evidence for Small-Amplitude Slow Domain Motions in a Multispanning Transmembrane α -Helical Protein. *J. Am. Chem. Soc.* **2017**, *139*, 9246–9258.
- (24) Legros, C.; Pollmann, V.; Knaus, H.-G.; Farrell, A. M.; Darbon, H.; Bougis, P. E.; Martin-Eauclaire, M.-F.; Pongs, O. Generating a High Affinity Scorpion Toxin Receptor in KcsA-Kv1.3 Chimeric Potassium Channels. *J. Biol. Chem.* **2000**, *275*, 16918–16924.
- (25) Shi, C.; He, Y.; Hendriks, K.; de Groot, B. L.; Cai, X.; Tian, C.; Lange, A.; Sun, H. A Single NaK Channel Conformation Is Not Enough for Non-Selective Ion Conduction. *Nat. Commun.* **2018**, *9*, 717.
- (26) Cortes, D. M.; Perozo, E. Structural Dynamics of the Streptomyces Lividans K⁺ Channel (SKC1): Oligomeric Stoichiometry and Stability. *Biochemistry* **1997**, *36*, 10343–10352.
- (27) Hyberts, S. G.; Milbradt, A. G.; Wagner, A. B.; Arthanari, H.; Wagner, G. Application of Iterative Soft Thresholding for Fast Reconstruction of NMR Data Non-Uniformly Sampled with Multi-dimensional Poisson Gap Scheduling. *J. Biomol. NMR* **2012**, *52*, 315–327.
- (28) Hyberts, S. G.; Takeuchi, K.; Wagner, G. Poisson-Gap Sampling and Forward Maximum Entropy Reconstruction for Enhancing the Resolution and Sensitivity of Protein NMR Data. *J. Am. Chem. Soc.* **2010**, *132*, 2145–2147.
- (29) Kazimierczuk, K.; Orekhov, V. Y. Accelerated NMR Spectroscopy by Using Compressed Sensing. *Angew. Chem., Int. Ed.* **2011**, *50*, 5556–5559.
- (30) Orekhov, V. Y.; Jaravine, V. A. Analysis of Non-Uniformly Sampled Spectra with Multi-Dimensional Decomposition. *Prog. Nucl. Magn. Reson. Spectrosc.* **2011**, *59*, 271–292.
- (31) Mayzel, M.; Kazimierczuk, K.; Orekhov, V. Y. The Causality Principle in the Reconstruction of Sparse NMR Spectra. *Chem. Commun.* **2014**, *50*, 8947–8950.
- (32) Delaglio, F.; Grzesiek, S.; Vuister, G.; Zhu, G.; Pfeifer, J.; Bax, A. NMRPipe: A Multidimensional Spectral Processing System Based on UNIX Pipes. *J. Biomol. NMR* **1995**, *6*, 277–293.
- (33) Skinner, S. P.; Fogh, R. H.; Boucher, W.; Ragan, T. J.; Mureddu, L. G.; Vuister, G. W. CcpNmr AnalysisAssign: A Flexible Platform for Integrated NMR Analysis. *J. Biomol. NMR* **2016**, *66*, 111–124.
- (34) Kopec, W.; Köpfer, D. A.; Vickery, O. N.; Bondarenko, A. S.; Jansen, T. L. C.; de Groot, B. L.; Zachariae, U. Direct Knock-on of Desolvated Ions Governs Strict Ion Selectivity in K⁺ Channels. *Nat. Chem.* **2018**, *10*, 813–820.
- (35) Bhate, M. P.; McDermott, A. E. Protonation State of E71 in KcsA and Its Role for Channel Collapse and Inactivation. *Proc. Natl. Acad. Sci. U.S.A.* **2012**, *109*, 15265–15270.
- (36) Berendsen, H. J. C.; van der Spoel, D.; van Drunen, R. GROMACS: A Message-Passing Parallel Molecular Dynamics Implementation. *Comput. Phys. Commun.* **1995**, *91*, 43–56.
- (37) Lindahl, E.; Hess, B.; van der Spoel, D. GROMACS 3.0: A Package for Molecular Simulation and Trajectory Analysis. *J. Mol. Model.* **2001**, *7*, 306–317.
- (38) Van Der Spoel, D.; Lindahl, E.; Hess, B.; Groenhof, G.; Mark, A. E.; Berendsen, H. J. C. GROMACS: Fast, Flexible, and Free. *J. Comput. Chem.* **2005**, *26*, 1701–1718.
- (39) Hess, B.; Kutzner, C.; van der Spoel, D.; Lindahl, E. GROMACS 4: Algorithms for Highly Efficient, Load-Balanced, and Scalable Molecular Simulation. *J. Chem. Theory Comput.* **2008**, *4*, 435–447.
- (40) Roux, B. The Membrane Potential and Its Representation by a Constant Electric Field in Computer Simulations. *Biophys. J.* **2008**, *95*, 4205–4216.
- (41) Gumbart, J.; Khalili-Araghi, F.; Sotomayor, M.; Roux, B. Constant Electric Field Simulations of the Membrane Potential Illustrated with Simple Systems. *Biochim. Biophys. Acta, Biomembr.* **2012**, *1818*, 294–302.
- (42) Hornak, V.; Abel, R.; Okur, A.; Strockbine, B.; Roitberg, A.; Simmerling, C. Comparison of Multiple Amber Force Fields and Development of Improved Protein Backbone Parameters. *Proteins: Struct., Funct., Bioinf.* **2006**, *65*, 712–725.
- (43) Huang, J.; Rauscher, S.; Nawrocki, G.; Ran, T.; Feig, M.; de Groot, B. L.; Grubmüller, H.; MacKerell, A. D. CHARMM36m: An Improved Force Field for Folded and Intrinsically Disordered Proteins. *Nat. Methods* **2017**, *14*, 71–73.
- (44) Furini, S.; Domene, C. Critical Assessment of Common Force Fields for Molecular Dynamics Simulations of Potassium Channels. *J. Chem. Theory Comput.* **2020**, *16*, 7148–7159.
- (45) Cordomí, A.; Caltabiano, G.; Pardo, L. Membrane Protein Simulations Using AMBER Force Field and Berger Lipid Parameters. *J. Chem. Theory Comput.* **2012**, *8*, 948–958.
- (46) Berger, O.; Edholm, O.; Jähnig, F. Molecular Dynamics Simulations of a Fluid Bilayer of Dipalmitoylphosphatidylcholine at Full Hydration, Constant Pressure, and Constant Temperature. *Biophys. J.* **1997**, *72*, 2002–2013.

- (47) Jorgensen, W. L.; Chandrasekhar, J.; Madura, J. D.; Impey, R. W.; Klein, M. L. Comparison of Simple Potential Functions for Simulating Liquid Water. *J. Chem. Phys.* **1983**, *79*, 926–935.
- (48) Joung, I. S.; Cheatham, T. E. Determination of Alkali and Halide Monovalent Ion Parameters for Use in Explicitly Solvated Biomolecular Simulations. *J. Phys. Chem. B* **2008**, *112*, 9020–9041.
- (49) Feenstra, K. A.; Hess, B.; Berendsen, H. J. C. Improving Efficiency of Large Time-Scale Molecular Dynamics Simulations of Hydrogen-Rich Systems. *J. Comput. Chem.* **1999**, *20*, 786–798.
- (50) Darden, T.; York, D.; Pedersen, L. Particle Mesh Ewald: An $N \cdot \log(N)$ Method for Ewald Sums in Large Systems. *J. Chem. Phys.* **1993**, *98*, 10089–10092.
- (51) Bussi, G.; Donadio, D.; Parrinello, M. Canonical Sampling through Velocity Rescaling. *J. Chem. Phys.* **2007**, *126*, 014101.
- (52) Berendsen, H. J. C.; Postma, J. P. M.; van Gunsteren, W. F.; DiNola, A.; Haak, J. R. Molecular Dynamics with Coupling to an External Bath. *J. Chem. Phys.* **1984**, *81*, 3684–3690.
- (53) Klauda, J. B.; Venable, R. M.; Freites, J. A.; O'Connor, J. W.; Tobias, D. J.; Mondragon-Ramirez, C.; Vorobyov, I.; MacKerell, A. D.; Pastor, R. W. Update of the CHARMM All-Atom Additive Force Field for Lipids: Validation on Six Lipid Types. *J. Phys. Chem. B* **2010**, *114*, 7830–7843.
- (54) MacKerell, A. D.; Bashford, D.; Bellott, M.; Dunbrack, R. L.; Evanseck, J. D.; Field, M. J.; Fischer, S.; Gao, J.; Guo, H.; Ha, S.; Joseph-McCarthy, D.; Kuchnir, L.; Kuczera, K.; Lau, F. T. K.; Mattos, C.; Michnick, S.; Ngo, T.; Nguyen, D. T.; Prodhom, B.; Reiher, W. E.; Roux, B.; Schlenkrich, M.; Smith, J. C.; Stote, R.; Straub, J.; Watanabe, M.; Wiórkiewicz-Kuczera, J.; Yin, D.; Karplus, M. All-Atom Empirical Potential for Molecular Modeling and Dynamics Studies of Proteins. *J. Phys. Chem. B* **1998**, *102*, 3586–3616.
- (55) Beglov, D.; Roux, B. Finite Representation of an Infinite Bulk System: Solvent Boundary Potential for Computer Simulations. *J. Chem. Phys.* **1994**, *100*, 9050–9063.
- (56) Hoover, W. G. Canonical Dynamics: Equilibrium Phase-Space Distributions. *Phys. Rev. A: At., Mol., Opt. Phys.* **1985**, *31*, 1695–1697.
- (57) Nosé, S. A Unified Formulation of the Constant Temperature Molecular Dynamics Methods. *J. Chem. Phys.* **1984**, *81*, 511–519.
- (58) Parrinello, M.; Rahman, A. Polymorphic Transitions in Single Crystals: A New Molecular Dynamics Method. *J. Appl. Phys.* **1981**, *52*, 7182–7190.
- (59) Kopec, W.; Rothberg, B. S.; de Groot, B. L. Molecular Mechanism of a Potassium Channel Gating through Activation Gate-Selectivity Filter Coupling. *Nat. Commun.* **2019**, *10*, 5366.
- (60) Fricke, P.; Chevelkov, V.; Zinke, M.; Giller, K.; Becker, S.; Lange, A. Backbone Assignment of Perdeuterated Proteins by Solid-State NMR Using Proton Detection and Ultrafast Magic-Angle Spinning. *Nat. Protoc.* **2017**, *12*, 764–782.
- (61) Sanders, J. K. M.; Hunter, B. K.; Jameson, C. J.; Romeo, G. Isotope Effects on Proton Chemical Shifts and Coupling Constants in the Ammonium Ions $15, 14 \text{ NH}_4\text{-ND}_n^+$. *Chem. Phys. Lett.* **1988**, *143*, 471–476.
- (62) Hendriks, K.; Öster, C.; Shi, C.; Sun, H.; Lange, A. Sodium Ions Do Not Stabilize the Selectivity Filter of a Potassium Channel. *J. Mol. Biol.* **2021**, *433*, 167091.
- (63) Lange, A.; Giller, K.; Hornig, S.; Martin-Eauclaire, M.-F.; Pongs, O.; Becker, S.; Baldus, M. Toxin-Induced Conformational Changes in a Potassium Channel Revealed by Solid-State NMR. *Nature* **2006**, *440*, 959–962.
- (64) Zhou, Y.; Morais-Cabral, J. H.; Kaufman, A.; MacKinnon, R. Chemistry of Ion Coordination and Hydration Revealed by a K⁺ Channel–Fab Complex at 2.0 Å Resolution. *Nature* **2001**, *414*, 43–48.
- (65) Ader, C.; Schneider, R.; Hornig, S.; Velisetty, P.; Vardanyan, V.; Giller, K.; Ohmert, I.; Becker, S.; Pongs, O.; Baldus, M. Coupling of Activation and Inactivation Gate in a K⁺-Channel: Potassium and Ligand Sensitivity. *EMBO J.* **2009**, *28*, 2825–2834.
- (66) Chakrapani, S.; Cordero-Morales, J. F.; Jogini, V.; Pan, A. C.; Cortes, D. M.; Roux, B.; Perozo, E. On the Structural Basis of Modal